International Journal of Heat and Mass Transfer 215 (2023) 124525

Contents lists available at ScienceDirect

International Journal of Heat and Mass Transfer

journal homepage: www.elsevier.com/locate/ijhmt

A quantitative study on the thermal performance of self-modified heat transfer surfaces in high heat flux flow systems

A. Sergis [a,*], Y. Hardalupas [a], K. Flinders [b], D. Hancock [b], T. Barrett [b]

[a] The Department of Mechanical Engineering, Imperial College London, London SW7 2AZ, UK
[b] Culham Science Centre, United Kingdom Atomic Energy Authority, Abingdon OX14 3DB, UK

ARTICLE INFO

Keywords:
HIVE
Fusion
Nanoparticles
Heat transfer
High heat flux
Deposition

ABSTRACT

The current work uses a novel fundamental heat transfer experiment to understand the morphological and thermal performance effects of nanoparticle deposition processes on heating surfaces under high heat fluxes. This is a unique fundamental study of nanosuspension induced nanoparticle coated boiling surfaces under realistic fusion relevant conditions. Al_2O_3—H_2O nanosuspensions have been used under forced convection and boiling. The experiments were performed on a test bed able to simulate realistic fusion reactor heat flux. Nanosuspensions are found to deteriorate the cooling performance due to the formation of a complex self-assembled porous nanoparticle layer on the heating surfaces. This negative effect on thermal performance is irrespective of operation in nanoparticulate latent or pure coolants modes. For heat transfer in nanosuspensions, the increase of nanoparticle concentration reduced the observed negative thermal performance effects. Improvement of thermal performance beyond the break-even point, as witnessed for some conditions in the current work, could be potentially achieved by increasing the concentration of nanoparticles in the coolant. When the nanosuspension is removed and the heat transfer surfaces with the nanolayer deposit are washed and operated with pure liquids, it was discovered that the deposited layers survived and still affected (negatively) their heat transfer performance. The deposited layers are porous and are expected to extend the critical heat flux of surfaces in relevant industrial processes. The deposition process and the final thermal properties could be affected by several controlled parameters providing design opportunities for new or retrofitted applications that were otherwise inaccessible or unfeasible.

1. Introduction

The need for sustainable and abundant energy supply as well as energy efficiency is more prominent than ever before. It is likely that the world will have to revise how it produces, handles, stores and uses energy in relation to its environmental impact whilst ensuring security of energy supplies. Development of heat transfer (and storage) technology will play a significant role in achieving these tasks because, in most applications, it defines the thermodynamic efficiency and/or the performance of the process in thermal power generation (micro/small/large scale) and in renewable energy storage. Heat management physics must be advanced to facilitate the development of new applications. This work aims to understand the physics of heat transfer in nanosuspensions and their subsequent effects on heat transfer surfaces.

An important heat transfer mode in power generation is through boiling of liquids (in most industrially relevant cases this is flow boiling of water). These processes are limited by the critical heat flux (CHF) point, which is affected by the flowing and thermal properties of coolants as well as by the texture and geometry of surfaces. Knowledge of CHF, or more specifically the setpoint of its operation, is widely important in safeguarding boiling applications and avoiding "burn out" i.e., the limiting heat flux a heat transfer surface can endure before getting destroyed by the resulting elevated temperatures. Surface modifications to improve boiling heat transfer processes is not a new concept. This has been widely investigated in the literature in the form of elaborate designs of hydrophobic and hydrophilic surfaces or more advanced biphilic patterned surfaces that can change boiling dynamics (including the onset and dynamics of boiling) as well as delay the CHF. For the latter, which is of current interest, a delay of the CHF up to ~200% utilizing such methods has been documented [1].

It has been shown that boiling surfaces operated in the presence of nanoparticle latent coolants develop self-assembled and self-healing

* Corresponding author.
E-mail address: a.sergis09@imperial.ac.uk (A. Sergis).

https://doi.org/10.1016/j.ijheatmasstransfer.2023.124525
Received 3 April 2023; Received in revised form 4 July 2023; Accepted 18 July 2023
Available online 22 July 2023

dynamic structures (nano/micro-layers) from suspended nanoparticles that can alter and enhance boiling dynamics. Such enhancements involve the delay of the CHF otherwise encountered with traditional coolants and heat transfer surfaces. Significant enhancements over the carrier fluid have been experimentally reported in the literature [2,3] albeit for pool boiling cases; for example 175% and 200% delay to the CHF in pool boiling has been reported experimentally by Kim et al. [4] and You et al. [5], respectively. Understanding the physics which give rise to these phenomena at the nanoscale and extrapolating those to flow boiling applications, will be important to the rational design of high-performance thermal devices such as future nuclear fusion reactors, small modular fission reactors, advanced high performance heat pumps as well as managing heat from high thermal energy density devices (e.g., electronics) and others.

The current work describes a realistic preliminary parametric high heat flux (HHF), forced convection and early onset of flow boiling heat transfer experiment to assess and quantify the potential of self-induced, boiling heat transfer surface modification using nanoparticle latent coolants as well as coolants with nanosuspensions. The experimental procedure aimed to focus on the pre and early onset of flow boiling performance of nanosuspensions to gauge their behaviour in such systems and guide future excursions, safely, into the hard and limiting CHF boiling regimes. The emerging modified surfaces have been thereafter rinsed and tested with pure, traditional coolants (in this case deionised water) to assess their thermal performance in the absence of nanoparticles inside the coolant itself. The parametric experiment provides evidence of the applicability of modified surfaces using nanosuspensions in high heat flux components that could justify their potential use in the International Thermonuclear Experimental Reactor (ITER) and the European DEMOnstration power plant (DEMO).

2. Methodology

This section documents the experimental apparatus, the subsequent nanoparticle suspension preparation method and materials as well as the parametric methodology boundaries and data processing used.

2.1. Experimental apparatus

The experiment took place at the Heat by Induction to Verify Extremes (HIVE) facility at UKAEA. This comprised of:

i. An instrumented test platform that was able to deposit fusion relevant heat loads onto samples in a vacuum chamber (see Section 2.1.1).
ii. A modular nanosuspension circulation loop that comprised of flow measurement and pumping apparatus to circulate the coolant in a safe and controlled manner (see Section 2.1.2).
iii. An instrumented test section (see Section 2.1.3) installed in the chamber and connected to the loop.

The type of suspensions and their manufacturing process is elaborated in Section 2.1.4 whilst the parametric study is detailed in Section 2.1.5. The test section sample used, as well as the HIVE facility, are described in detail by the work of D. Hancock et al. (2018) [6]; as such, a shortened description is provided for these in the current section.

2.1.1. Heat by induction to verify extremes (HIVE) rig

The HIVE test rig located at CCFE offers a flexible, low-cost method for the testing of small prototype components at high heat fluxes (HHF). The system works on the induction heating principle, whereby a pancake coil operating at high frequency induces a mirror current on an armour surface, heating the sample, in this case a tungsten tile on a copper cooling block, via the joule effect. This heating, to a penetration depth of <1 mm, resulted in a maximum temperature rise of approximately 1500 °C.

The HIVE rig consists of a 50–150 kHz, 45 kW induction heating system able to inductively heat the test section with an efficiency of ~30–40% and a penetration depth of <1 mm. The inductive coils and test section are placed inside an evacuated vessel capable of fusion relevant vacuum pressures down to $\sim 10^{-7}$mbar. A 35 kW water cooling system, comprised of 2 chillers and a temperature control unit (TCU), the vacuum vessel, and various diagnostics are used to set and control the boundary conditions of the experiment. The HIVE cooling system needs to be isolated from the nanosuspension experiment to minimise any effects of nanoparticle contamination that might affect unrelated future experimentation on the facility. As such, the nano colloid suspension loop was physically decoupled from the HIVE cooling system via a heat exchanger and interfaced to it only with control and instrumentation (C&I) and through the test section connections and pipework.

2.1.2. Nanosuspension loop and its coupling to HIVE

The nanosuspension cooling loop is designed to incorporate its own independent electromechanical components which are interfaced with the plant control systems for HIVE. A block diagram of the components can be seen in Fig. 1. The nanosuspension loop is operated at atmospheric pressure via an open to air header tank. The header tank is used for nanosuspension dosing throughout the experiment via a recirculation pump. The flow rates of the nanosuspension loop can be controlled as per the requirements of the experiment.

Active and passive safety control mechanisms are used governing the nanosuspension rig operation and its interfacing with HIVE. For example, electronic pressure transducers are interfaced with the control system of the rig, as well as that of (HIVE), to detect potential leaks (low pressures) or overpressures (e.g., uncontrolled boiling). Additional electronic and information coupling busses governing the start-up, transient, steady state and shutdown sequences of each of the two facilities has been accommodated. The systems facilitate selective and automatic deactivation of certain components of both the HIVE plant and the nanosuspension loop to allow safe and automatic procedures to take place as well as prevent out of design scenarios to initiate and/or develop that might endanger damaging equipment and potentially injuring personnel.

Other than the electromechanical connections, the nanosuspension loop connects hydraulically with HIVE at two points:

i. At the HIVE chiller manifolds via the use of a counterflow heat exchanger and header tank used to reject heat from the nanosuspension whilst keeping it isolated from the remaining hydraulic components of HIVE (to avoid nanoparticle contaminants into the test bed hydraulic systems). The recirculating nanosuspension flow passes through a heat exchanger which is connected to a 15 kW chiller provided at HIVE to facilitate isolation of the nanosuspension loop with the deionised water supply loops used for HIVE.
ii. At the nanosuspension vacuum vessel delivery and return manifolds that lead to the test section. The nanosuspension loop delivers a measured flow to the test sample (test sample loop) inside the HIVE Vessel.

The key features of the nanosuspension circulation loop are as follows:

i. A counterflow liquid to liquid heat exchanger (chiller primary coolant loop to nanosuspension) with a cooling capacity of 22 kW. This controls the temperature of the bulk nanosuspension loop up to 90 °C. The header tank incorporates an automatic pressure relief control valve that sustains atmospheric pressure in the tank. The valve exhaust into a catch tank to make sure that any nanoparticle latent liquid is contained in case of unexpected global pressure rise within the unpressurised components.
ii. The hydraulic interfacing is performed through female/male “Staubli” brand quick connectors. Flexible tubes connect the

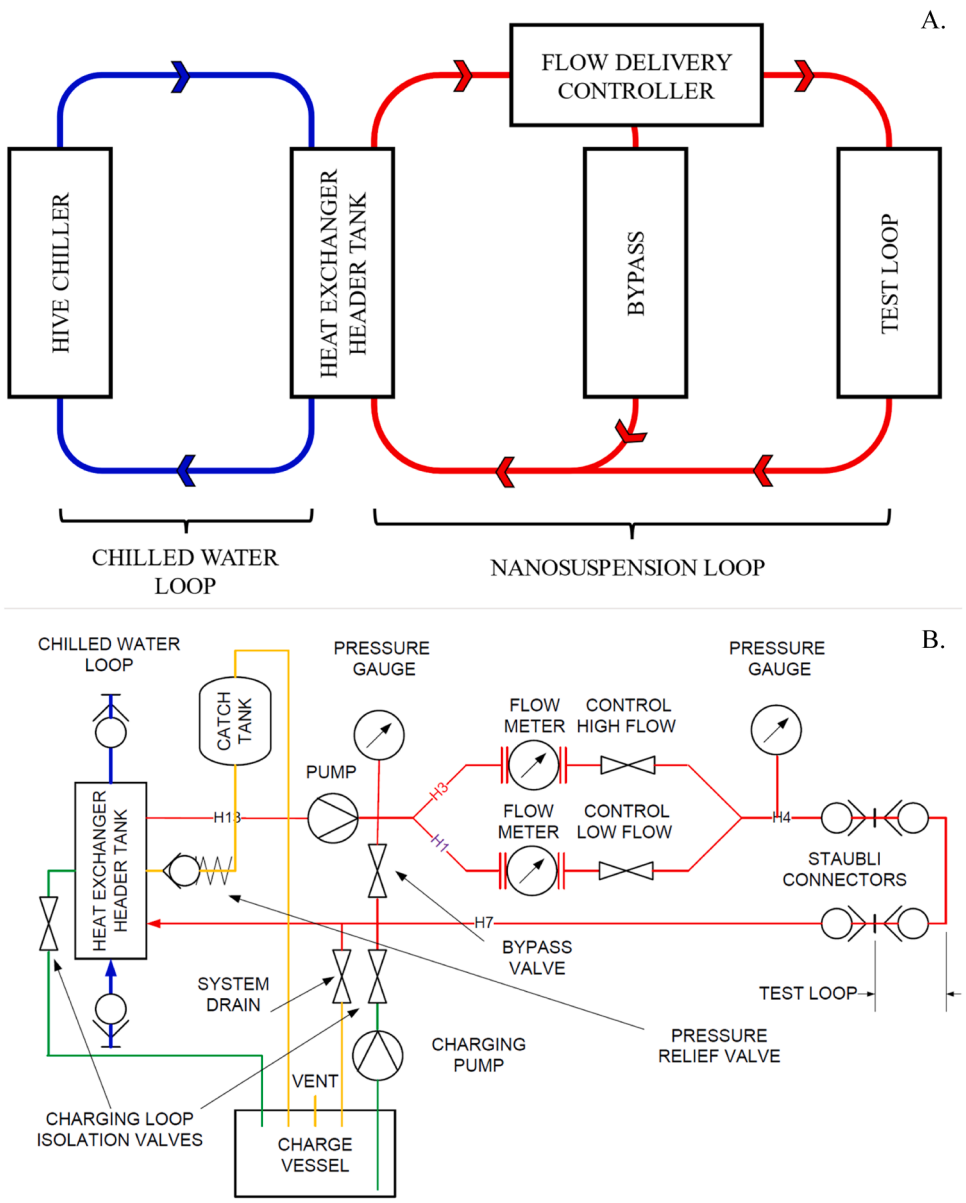

Fig. 1. Nanosuspension hydraulic component schematic and their thermohydraulic interfacing to HIVE. A. Simplified block diagram of main components and primary working fluid pathways and B. Detailed hydraulic schematic of rig. For both diagrams, red colour represents the nanosuspension loop, in blue colour the isolated HIVE chiller water loop, in green colour the nanosuspension charging paths and in yellow colour are the nanosuspension drain and overpressure drain and vent paths.

chiller to the heat exchanger and the nanosuspension loop to the manifolds of the vacuum vessel (leading to the test section).

iii. Two pumps are installed; a main pump to control the main flow of nanosuspension and a secondary drain pump. The main pump provides a variable flow rate of up to ~2.5 kg/s of water. The drain pump is used to recirculate the nanosuspensions between the header tank and main loop (for the purpose of nanoparticle mixing) as well to empty and refill the loop.

iv. Stainless steel components are used throughout the hard piped sections of the loop. This includes the header tank. The header tank incorporates a drain, filler cap and water level indicators. The drain pump is connected to the header tank via a valve.

v. Electromechanical interface coupling and control systems.

vi. Flow and pressure indicators are installed as per Fig. 1. The flow meter uncertainty was 1%.

vii. A drip tray is included at the base of the loop to contain leaks.

2.1.3. Test section sample

The sample used is the same as the "AMAZE commissioning sample" detailed in the work of D. Hancock et al. (2018) [6]. This consists of an Oxygen-Free High thermal Conductivity (OFHC) copper block (30 mm x 20 mm x 50 mm) brazed to a 30 mm x 30 mm x 5 mm tungsten armour. Tungsten is used because it is the preferred plasma facing material for most divertor concepts. Copper feed tubes (10 mm in internal diameter) are brazed internally to the copper block and are used to circulate the coolants. The tungsten armour is facing the induction coil hence the heat flux direction is expected to move at a plane perpendicular to the armour and into the copper block. The heat flux profile is more intense towards the edges of the tungsten armour and lower at the middle of the armour [6]. A cross-section of the test sample can be found in Fig. 2.

Seven K-type thermocouples have been embedded inside the copper block section (using percussion welding inside drilled pockets of the copper block) and the external surfaces of the inlet and outlet feeding tubes. The thermocouples were interfaced with the measurement and

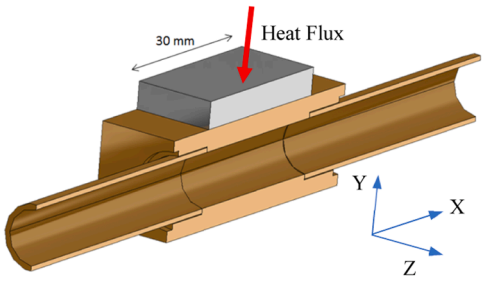

Fig. 2. Test sample cross-section, in bronze colour depicting the OFHC copper parts and in grey colour the tungsten armour [6]. The heat flux direction is indicated by the red arrow.

command module of HIVE. The location of the thermocouples can be found in Fig. 3. Please note that the inlet, In 1&2, as well as the outlet, Out 1&2, thermocouples are offset by 90° Subsequently another three thermocouples are installed to monitor the test section spatial temperatures as follows: one at the top heat flux facing side of the test section, noted as top inlet face (Tif), top mid face (Tmf) and top outlet face (Tof).

Redundant thermocouples are installed not only for validation and spatial measurement purposes but also for practical aspects in the case of failures, magnetic pulse interferences as well as burnouts from the harsh environment due to the inductive heating process (high failure tolerance is required in this example as the manufacturing of the sample as well as the conduct of the experiment would not have allowed easy access for repairs). Indeed, upon commissioning the loop and testing, it was discovered that the thermocouples validated as successfully providing measurements across the range of boundary conditions tested were In 1, Out 2 and Tmf. The rest of the thermocouples suffered from the following:

i. In 2 – minor interference from coupling with the electromagnetic (EM) pulses across the range of boundary conditions was recorded. It was decided to omit altogether the readings to ensure that the results recorded were not affected.
ii. Out 1 – burnout likely due to inductive coupling with the EM pulse providing no values.
iii. Tif – minor high frequency irregular oscillations were induced in the temperature signal for some heat fluxes tested (the power delivery was performed through modulated frequency pulses) due to partial resonant coupling with the driving EM coil as well as slower response for other non-resonant frequencies believed to be a result of unsuccessful thermal coupling with the material surface. It was decided to omit the readings from the bulk results to ensure their clarity and accuracy however, the readings can be used indicatively for trend validation purposes outside the interference range.

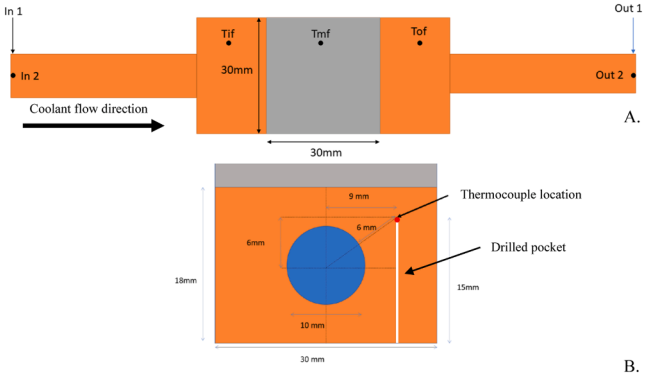

Fig. 3. A. top down and B. cross-sectional view [6] of test sample indicating thermocouple locations. In orange colour are the copper components, in grey colour the tungsten armour and in blue the coolant flow passage.

The uncertainty of the recording system for the temperature measurements was ≤0.1 K for the reported results.

In the absence of a fluid mixing chamber and the, intentionally, non-uniform heating profile of the flowing coolant inside the feeding tubes the inlet and outlet thermocouples could only be used for validation purposes rather than a quantification of the heat flux absorbed by the coolant at steady state. To determine the absorbed heat flux by the coolant at steady state, calibration experiments have been performed that allowed the calculation for this directly from the input electrical power to the induction coils.

2.1.4. Nanosuspension preparation

The two-step method of nanosuspension preparation was used to compose the final mixtures used for the experiment. This involved mixing dry nanoparticle powders into deionised water and following a recommended set of mixing processes as those are commonly used in the field. Dense Al_2O_3—H_2O (50 nm particle size nanoparticles sourced from Alfa Aesar Stock No. 044931, CAS no. 1344-28) mixtures were composed at Imperial College and transferred to UKAEA inside capped glass test tubes. No surfactant was used in the preparation of nanosuspensions for this experiment as generally surfactants display unpredictable behaviours at elevated temperatures (i.e., above ~60°C). Previous stability studies by the same authors quantified the stability and quality of suspension of the formulated nanosuspensions in the absence of a surfactant [7,8]. The experimental process was also short (<10 h) in a high shear environment imposed by the flow circuit used. On the day of the experiment, the samples were agitated using a vortex mixer and then placed inside an ultrasonic bath (Guyson Kerry MKC14) for at least 5 hrs before experimentation. The dense solutions were thereafter agitated once more. A measured amount of deionised water was used to fill up the nanosuspension loop. The final dense nanosuspensions were emptied inside the header tank of the nanosuspension loop to form the prescribed mixtures listed in Table 1 after which the charging and main pumps were used to circulate the nanoparticles inside the coolant loop and achieve the targeted dilution.

2.1.5. Parametric study

The experiment aimed to answer a list of hypotheses for the forced convection and flow boiling conditions as a preliminary step to this endeavour. CHF extension points were not tested under this experimental excursion but are planned as part of future work through the offered understanding from the current results. The specific parametric study in the current work attempts to address the following preliminary hypotheses for experimentation with dilute nanosuspensions:

A. *Nanoparticles affect cooling performance of forced convection and early onset of flow boiling processes (i.e., well before limiting boiling conditions occur)*:
   A quantification of the thermal performance of forced convection and onset of boiling (early onset of flow boiling) would be attempted.
B. *A self-assembled nanoparticle layer (SANL) forms on heating surfaces which might affect their thermal performance*:
   An investigation to understand the topology and characteristics of the layer is attempted under forced convection and early onset of flow boiling conditions.
C. *The SANL and its effects persist even if the nanosuspension is removed and the heat transfer surface is operated with pure liquids*:
   Thermal quantification of the loop operating with pure liquids after the nanoparticle layer deposition is performed and the results compared to those when the loop was operating with nanosuspensions. The thermal effects of nanoparticles in the bulk coolant and those forming the SANL is quantified.

Table 1
Parametric study - order of experimental runs.

Order of group experimentation	Nanoparticle concentration φ /(% vol.)		Heat flux /(MW/m^2)					Set flow rates /(L/min)		
			P1	P2	P3	P4	P5	F1	F2	F3
1	Φ1	0.00*	1.50	2.25	3.00	3.75	4.50	5	10	18
2	Φ2	0.06								
3	Φ3	0.11								
4	Φ4	0.40								
5	Φ5	0.00*,^								

* Deionised water runs.
^ Run performed after loop was emptied from the nanosuspension and rinsed with deionised water before refilling and running with deionised water.

The thermocouple acquisition rate was set to 10 Hz whilst the heat flux pulse duration was set to 120 s. The inlet temperatures to the test section varied between 23 and 27 °C (i.e., strong subcooled flow) upon calibration (and later confirmed through the experiment). The inlet temperature to the test section appeared to drift for a max of ~4 °C during each of the 120 s pulses as a response to the transiently absorbed heat flux and limited capacity to reject all of this in a single fluid pass through the coupled heat exchanger.

Three nanoparticle volumetric concentrations (φ) and two runs without nanoparticle loadings i.e., using deionised water, were performed under five heat flux levels (delivered power levels) and three set flow rates. For the last run with deionised water, the loop was rinsed once with deionised water and the generated wastewater was discarded before refilling the loop with fresh deionised water and running the experiment.

The experimental runs were split into five groups, i.e., according to the particulate loading of the coolant, each containing 15 subgroup measurements (heat flux and flow rate combinations) in the order presented in Table 1. All heat flux and flow condition combinations have been executed for each nanoparticle loading before advancing to the next one. As such, data from a total of 75 runs was collected accordingly.

The pipe Reynolds number (Re_D) of the deionised water flow for the combinations of expected bulk temperatures and volumetric flow rates used is expected to lie within the range $1.1 \times 10^4 < Re_D < 1.3 \times 10^5$, which is larger than the transition to turbulence Re_D of 10^4; as such the flow of deionised water in the pipe remains turbulent. The thermal and hydrodynamic transition lengths are ten pipe diameters i.e., in this case 10 cm. Straight, unheated, sections of pipe, longer than the development length of the flow, are accommodated at the inlet and outlet to the heated test sections. As such, the state of the flow at the entrance of the heated test section is turbulent, and hydrodynamically developed. The heated part of the test section is shorter than the thermal development length of the flow (i.e., smaller than 10 cm) due to size limitations of the vacuum vessel and its thermal power output. As such, the thermal boundary layers are in a developing state within the entire length of the heated section of the test section. The flow regiment is hence complex and a straightforward method/correlation for calculating Nu_D to describe does not exist. A publication by Taler [9] provides more information into the complexity of such flows which goes beyond the scope of the current work. For reference, the estimated pipe Nusselt number (Nu_D) of the deionised water flow for the combinations of expected bulk temperatures and volumetric flow rates used is expected to lie within the range $80 < Nu_D < 360$ for the case of turbulent, fully developed (hydrodynamically and thermally) flows.

Experimental limits have been set conservatively to safeguard the equipment and personnel as the thermal behaviour of the suspensions or/and coatings formed on the heating surfaces might behave in an unpredictable manner.

2.1.6. Results processing

Numerous data points (of the order of 1×10^7) have been collected describing the performance of the sample and control parameters of HIVE and the coupled nanosuspension loop. An automated code was hence composed on MATLAB to automatically detect the onset and outset of pulses, determine suitable quasi steady regions within the pulses to select appropriate data points for processing and subsequently conditioning and postprocessing the signals to validate and generate the results presented. As such, for each pulse delivered an average temperature of interest was produced after filtering and conditioning the data.

To compensate for the temperature drift at the inlet of the test section (see Section 2.1.5) as well as minor target flow setting changes between runs (ranging to <1 L/min), the instantaneous temperature rise of the target thermocouple to the instantaneous inlet temperature was used, ΔT_{mf} (K), normalised by multiplying it with the product of the mass flow rate, $\dot{m}(\mathrm{kg/s})$, and thermal capacity, Cp_m (J/kgK), of liquid for each run. The $\dot{m}$ was calculated by multiplying the mixture density, $\rho_m(kg/m^3)$, with the volumetric flow rate of the liquid, $V(\dot{m}^3/s)$. The rule of mixtures has been used to calculate ρ_m and Cp_m. Eqs. (2.1) and (2.2) were hence used.

$$\dot{m} = \rho_m \dot{V} \tag{2.1}$$

$$\Delta T_{mf} = \left(T_{mf} - T_i\right)\dot{m}Cp_m \tag{2.2}$$

At least 1000 instantaneous data points for T_{mf} and ΔT_{mf} have been used to generate the average temperature results presented for each pulse (i.e., $\overline{T_{mf}}$ and $\overline{\Delta T_{mf}}$ respectively).

3. Results and discussion

Thermal performance results and characterisation of the nanoparticle layer is performed in the current section.

3.1. Thermal performance results

A SANL is observed on the heat transfer surfaces of the inner feed tube that persists (and in extend its thermal effects persist) even when the loop is rinsed with deionised water and thereafter operated with deionised water (more on that in Section 3.2). The focus of the comparative study was on Tmf. An absolute $\overline{T_{mf}}$ plot vs heat flux can be found in Fig. 4. Due to the proximity of Tmf to the feed tube and the high thermal conductivity of copper (see Fig. 3), we can assume that the temperature of the feed tube inner wall to have a small difference to that for Tmf. From the absolute $\overline{T_{mf}}$ plot it is evident that the inner surface of the tube does not exceed saturation temperatures for water (i.e., 100 °C) for some combinations of heat fluxes and flow rates. For example, for condition F3 (the highest flow rate) temperatures higher than the saturation temperature are only achieved for two points. The number of points having a temperature equal or higher to saturation increase as the flow rate decreases (as expected). Forced convection heat transfer is expected to dictate the points operating under saturation temperature whilst early onset of flow boiling characterizes the points equal and over the saturation temperature recorded. Indeed, across the same nanoparticle loading runs (i.e., for a nanoparticle loading run under varying heat flux and flow rate) it is evident from Fig. 4 that for most points

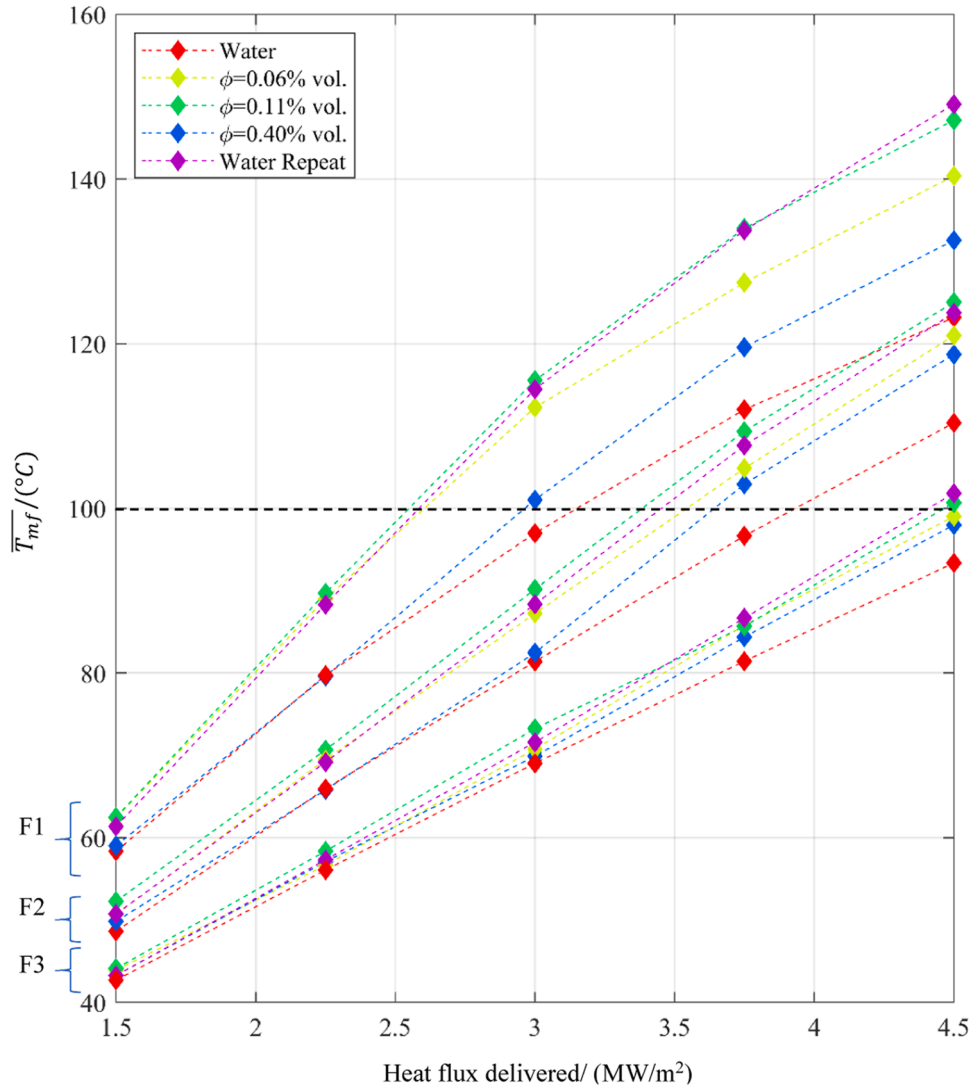

Fig. 4. $\overline{T_{mf}}$ evolution for different flow rates against heat flux. Please note that the sets of flow rates tested are represented by F1–3 as per Table 1. The dashed coloured straight joining lines are added to help the reader follow the nanoparticle loading families and do not necessarily represent a true depiction of the temperature trendline between the recorded points. The black dashed horizontal line marks the saturation temperature of water at atmospheric pressure.

operating under the saturation temperature, a linear relationship seems to be governing the temperature evolution with heat flux for different flow rates (as classically expected for forced convection heat transfer) whilst for points operating above the saturation temperature, linear relationships no longer seem to describe this (i.e., a variable and decreasing gradient is observed thereafter) which is characteristic of the change of mode of heat transfer to boiling (as expected).

The normalized results (i.e., $\overline{\Delta T_{mf}}$ against heat flux, Fig. 5) present a clearer behaviour for $\overline{T_{mf}}$ as the effects of mass flow rate deviations from the target flow rates in Table 1 and Ti temperature drifts (see Section 2.1.5) are compensated for. In addition, compensation has been applied for the small deviations between the different mixture Cp_m experimented with (due to the addition of Al_2O_3). Please note that the order of the flow family sets is reversed compared to Fig. 4. The following points can be deduced:

i. A similar behaviour is observed to the absolute $\overline{T_{mf}}$ trends where linear relationships seem to be describing the evolution of $\overline{\Delta T_{mf}}$ in forced convection but a varying and decreasing gradient is observed as the operation enters the early onset of flow boiling region.
ii. Generally, the operation of the loop with nanosuspensions as well as deionised water with a self-assembled nanolayer, behave worse than pure liquids for the forced convection and early onset of flow boiling regimes. This is indicated by the higher $\overline{\Delta T_{mf}}$ observed compared to those of deionised water in the absence of a SANL. It is not clear if this effect, can cause an early or delayed onset of boiling from the current results especially when considering the complexity of the deposited layer (see Section 3.2).
iii. Increasing nanoparticle concentrations in the suspensions seems to be improving their thermal behaviours especially when experiencing higher absolute temperatures (i.e., moving away from forced convection and entering the boiling regime). For the F1 flow family, the deionised water run in the absence of a SANL matches that of the nanosuspension run with the highest nanoparticle concentration. Further increase of nanoparticle concentration in the suspensions is likely to eventually lead to a superior coolant operated under the conditions tested.
iv. The deionised water runs with the SANL are generally behaving thermally worse than any of the other runs:
    - Starting from the deionised water runs with and without the presence of a SANL; the SANL seems to be deteriorating both,

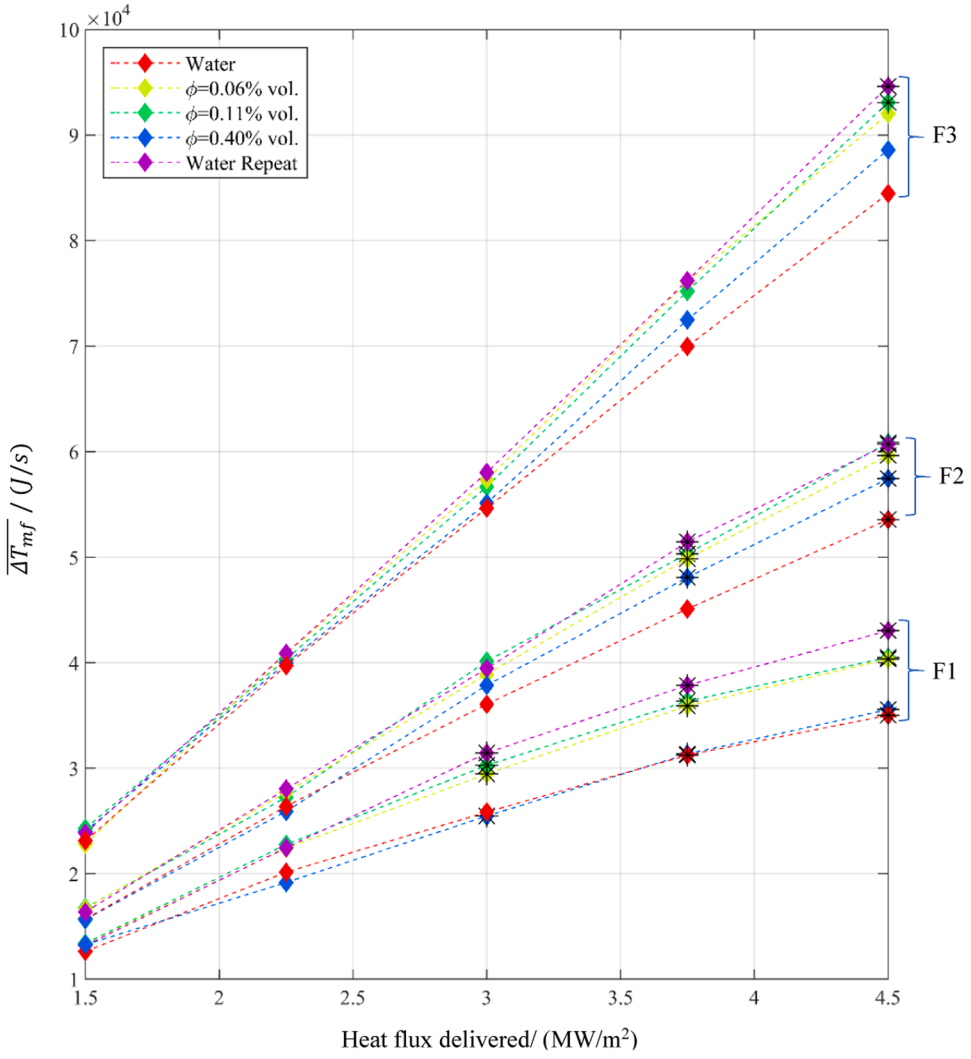

Fig. 5. $\overline{\Delta T_{mf}}$ evolution for different flow rates against heat flux. Please note that the sets of flow rates tested are represented by F1–3 as per Table 1. The dashed coloured straight joining lines are added to help the reader follow the nanoparticle loading families and do not necessarily represent a true depiction of the temperature trendline between the recorded points. Starred points mark those points reaching or/and exceeding the saturation temperature of water at atmospheric pressure.

forced convection and early onset of flow boiling heat transfer. The deposited material on the heat transfer surface is expected to deteriorate the overall heat transfer conduction coefficient through the solid surface which should eventually give rise to a higher $\overline{\Delta T_{mf}}$. A simple order of magnitude calculation can indicate if this is the case. The thermal conductivity of OFHC copper is ~30 times larger than the thermal conductivity of solid Al_2O_3 (for the sake of simplicity the SANL is assumed to be made from solid Al_2O_3). In addition, a conservative estimate places the thermal pathway distance in the OFHC to the feed tube (6 mm) versus the thermal pathway distance through the SANL (using a safe upper estimate of ~100 μm) to about ~60 times larger. As such, the thermal resistance of the OFHC pathway is approximately twice that of SANL (i.e., of the same order). The effective total thermal resistance through both, the OFHC and the SANL hence becomes approximately 1.5 times larger than before (i.e., without the SANL) and this could explain up to some degree the increase of the $\overline{\Delta T_{mf}}$ observed. Of course, the SANL is a complex porous layer which will also eventually affect the convective and boiling heat transfer coefficients however, the simple analysis above still provides an idea of the significance of deposition effects alone especially for the single phase/early onset of flow boiling cases (see Section 3.2).

- Carrying on to the comparison between the thermal performance of the nanosuspension runs against the deionised water runs in the presence of a SANL; the thermal performance of a SANL in the presence of a nanosuspension is better than that with deionised water. If it is assumed that the morphology and consistence of the SANL remains approximately the same between these runs, the improved behaviour can be attributed to an improved combined thermal performance of the bulk nanosuspensions and the layer (i.e., the layer continues to deteriorate the heat transfer coefficient in the same way but the nanosuspensions themselves behave thermally better than deionised water). It is unlikely that the SANL has had significant morphological changes between the nanosuspension runs and the deionised water runs thereafter (if this were the case, fluid flow shear and boiling effects would have removed this); but even if this were the case, it would have been expected that a thicker SANL might have been present during the nanosuspension runs compared to that without them. According to the previous argument, a thicker SANL would have deteriorated the overall heat transfer coefficient for the cases tested more, which strengthens the argument that the bulk nanosuspensions do improve the combined heat transfer performance observed.

Finally, a few comments with regards to the convective heat transfer

coefficient during single phase heat transfer (forced convection) in the presence of a SANL. From the current experiment it is not possible to understand whether the convective heat transfer coefficient of the pure or nanosuspension improves or deteriorates since the temperature measurement location inside the solid is affected by the added thermal resistance of the SANL itself. The results recorded hence present a coupled view of the (detrimental) thermal conductivity effects of the SANL and the (perhaps beneficial) effects of the convection coefficient. The convective coefficient itself and its evolution is difficult to understand with the current experiment. This is because the convective coefficient is itself coupled to both, the thermal properties of the liquid and its interaction with the surface (i.e., momentum and thermal boundary layers). These parameters can be affected by the presence of nanoparticles (for the nanosuspension tests) and the roughness/morphology of the SANL (both in the nanosuspension and pure liquid tests).

3.2. Self-assembled nanoparticle layer morphology

The test sample (see Fig. 6) has been sectioned along its axes of symmetry in the X-Z and Y-Z planes to allow optical access after the end of the experiment. A SANL has been observed on the heating side of the feed tube but not on the opposite side as this is evident in Fig. 6. The SANL is only visible on the side of the feed tube (designated in the image as "Top") where the heat flux entered the sample whilst it is absent from the opposite surface (designated as "Bottom"). Please note that the sample was loaded sidewise inside the vacuum vessel hence the heat flux vector was perpendicular to the gravitational pull vector. There is hence conclusive evidence that the SANL formation is driven by the presence of a heat flux. High magnification optical and scanning electron microscopy imaging have been performed on the top and bottom feed tube sample surfaces (see Fig. 7). The images confirm the presence of a porous

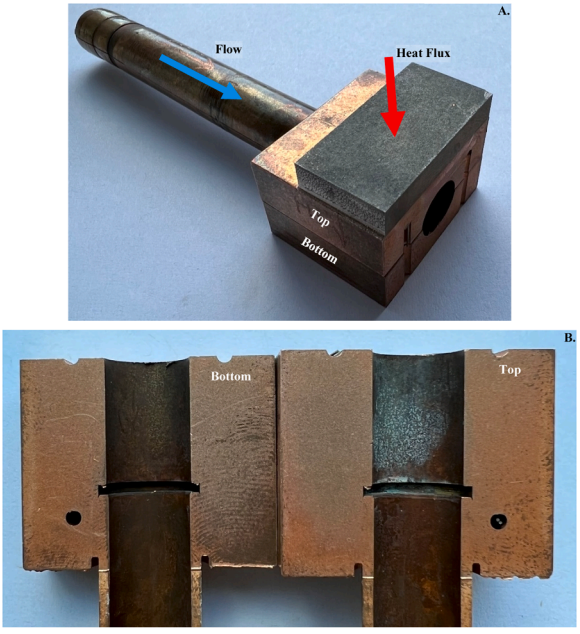

Fig. 6. Test sample orientation and cross-section photographs. In bronze colour depicting the OFHC copper parts in grey colour the tungsten armour. The cylindrical holes visible represent the thermocouple holes. A. Assembled test sample indicating the Y-Z cut plane with "Top" indicating the piece facing the heat flux and "Bottom" indicating the piece facing away from the heat flux direction as currently depicted (please note that the sample was loaded sidewise inside the vacuum vessel hence the heat flux vector was perpendicular to the gravitational pull vector). The heat flux and flow directions are indicated by the red and blue arrows respectively. B. Y-Z and X-Z plane sectioned sample showing internal coolant flow surfaces. The white speckle of the top piece is the Al_2O_3 SANL.

layer which forms on the top sample surface. Integral surface spectroscopic measurements have been performed for characteristic areas of the top and bottom sample surfaces. These have concluded that the SANL is made of elemental aluminium and oxygen, i.e., the main constituents of Al_2O_3. The formation of the layer is interesting, it can be observed (confirmed via spectroscopy) that the layer is not uniformly covering the heating surface but instead forms networks of depositions with some areas of the heating surface left uncovered and others fully covered. This opens the potential of achieving patterned surfaces on heating surfaces, i.e., areas that can present different affinity to water with hence modified thermal characteristics. Literature already indicated that traditionally manufactured biphilic surfaces hold the potential of increasing CHF by 200% [1]. Understanding the controlled deposition mechanisms of particles on heating surfaces can lead to the formation of a desired biphilic SANL with superior thermal performance.

The SANL appears porous in the optical and scanning electron microscopy images. Even though the current investigation did not approach limiting boiling conditions the self-assembled structures are nevertheless expected to improve certain CHF characteristics. This is achieved through mechanisms which increase hydration of dry areas on the heat transfer surface under high heat flux conditions and hence delay dry out (burn out) effects close to the limiting CHF points. The effects are expected to be dynamic (temporal and spatial evolution) and can be potentially controlled by secondary nanosuspension mixture and operational condition properties (such as nanoparticle type, concentration and physical properties, suspension boiling time and heat flux etc.). Past research indicated that synthetic nanostructures on heating surfaces, like the SANL, have the potential of enhancing pool boiling heat transfer by delaying CHF points through the employment of similar CHF enhancing mechanisms as those encountered in the current experiment [10,11]. Such manufactured structures can be created by e.g., electroplating [1] and could be optimised according to the required porosity and density of nanostructured sides. These fabricated surfaces bare morphological similarities with the SANL observed in the current work and might be further augmented by potentially controlling the nanoparticle deposition process to lead to a patterned biphilic boiling surface. It is indeed interesting to explore the idea of designed SANLs and their dynamic evolution in the optimization of heat transfer surfaces for such applications which will be the subject of future work.

4. Conclusions

The current work focused on understanding the preliminary behavior of surfaces operating with and without nanosuspensions in the forced convection and early onset of flow boiling regime. A relevant to fusion experiment was conducted making use of the HIVE rig at CCFE UKAEA. The current work is a precursor to a series of experiments examined to understand whether the use of nanosuspensions could improve flow boiling heat transfer processes by extending the current conventional thermal operating limits of their heat exchanging surfaces.

Through the current experimentation excursion and its boundary conditions, an assessment of the hypotheses set at the onset of this work is evaluated:

A. *Nanoparticles affect cooling performance of forced convection and early onset of flow boiling processes (i.e., well before limiting boiling conditions occur)*:

The current research showed that this hypothesis holds true. Nanosuspensions behave generally worse than pure liquids through the boundary conditions tested. However, it is likely that bulk coolant improvement is achieved when boiling surfaces operate with nanosuspensions in the absence of deposited nanoparticle material on them.

B. *A self-assembled nanoparticle layer (SANL) forms on heating surfaces which might affect their thermal performance*:

A complex porous SANL did form on the heat exchanging surface

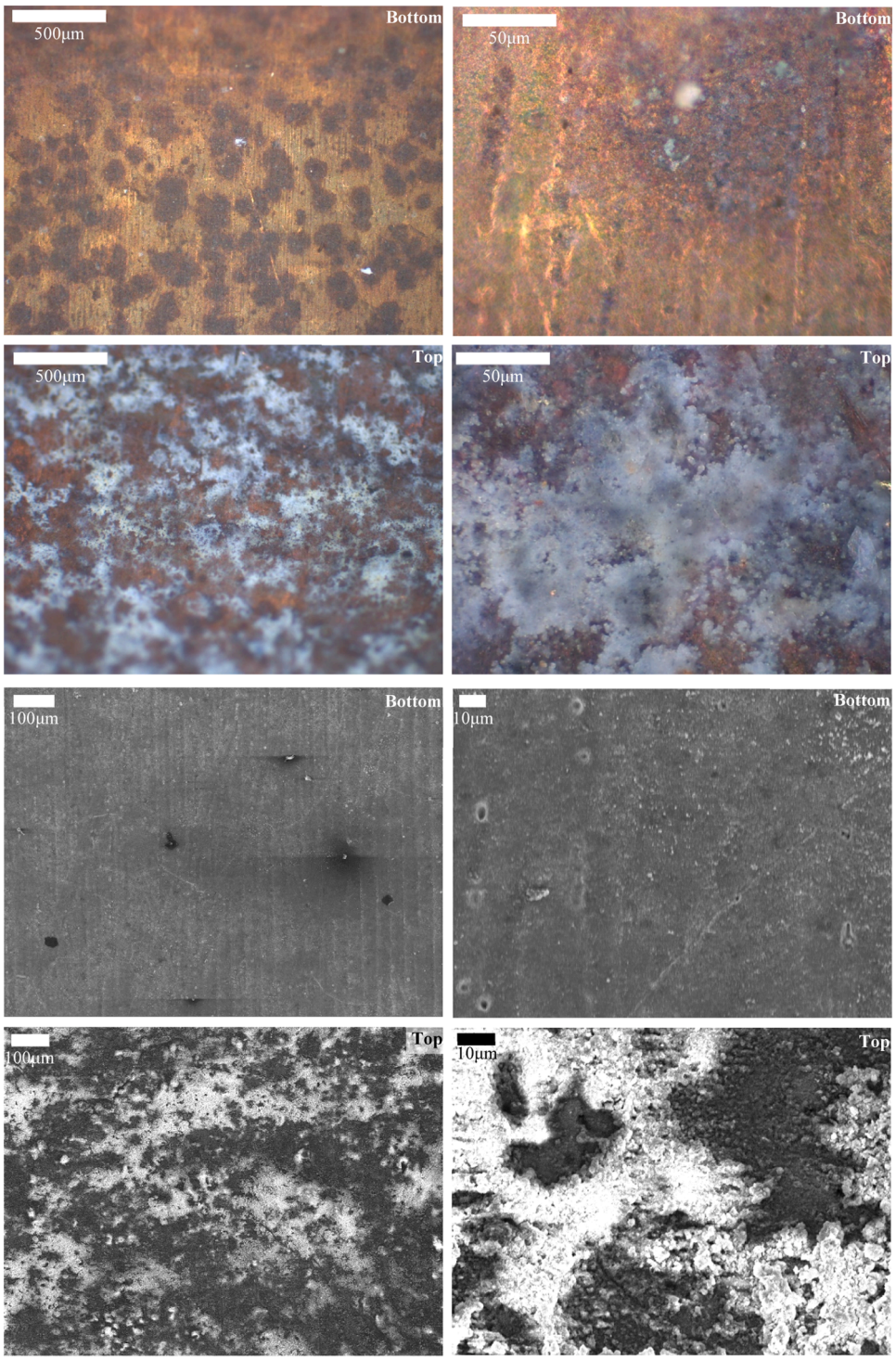

Fig. 7. The first two rows in the image matrix contain an optical microscopy image of the bottom (first row) and top (second row) sections of the sample. The last two rows of the image matrix contain scanning electron microscopy (SEM) images of the bottom (third row) and the top (fourth row) sections of the sample. The presence of the SANL is evident in the imaging of the top section of the sample (white coloured deposit).

that affects (generally in a negative way) their thermal performance in the heat transfer regimes tested (i.e., forced convection and early onset of flow boiling). A trend became clear indicating that increasing nanoparticle content in the nanosuspension reduced the negative thermal performance effects (up to the limits tested) when boiling surfaces with a SANL were operating in nanosuspensions. Addition of more nanoparticles in the solution might cause improvement of thermal performance beyond the break-even point witnessed in the current work.

C. *The SANL and its effects persist even if the nanosuspension is removed and the heat transfer surface is operated with pure liquids*:

This hypothesis was also found to be true. Deterioration of the thermal performance of boiling surfaces covered with a SANL in pure liquids was observed. In addition, it was found that the bulk nanosuspension thermal performance acts to negate the negative effects

caused by the SANL. This is because the heat transfer resistance of the SANL was found to be comparable to that of the OFHC material between the comparison thermocouple point and the coolant.

Generally, it is expected that the porous SANL could potentially delay the CHF which is of industrial interest in new and retrofitted applications with or without the presence of nanosuspensions as coolants. The negative effects of the lower heat transfer performance of the SANL at the forced convection and early onset of flow boiling regimes observed could be potentially negated by the operation of such SANL covered surfaces with denser nanosuspensions, than those examined in the current work, if such operation is deemed critical for a given application. The capacity to deploy designed SANLs and their ability to repair themselves is certainly an enticing option for boiling heat transfer applications which could be the subject of future work.

CRediT authorship contribution statement

A. Sergis: Conceptualization, Methodology, Software, Validation, Formal analysis, Investigation, Resources, Data curation, Writing – original draft, Writing – review & editing, Visualization, Project administration, Funding acquisition. **Y. Hardalupas:** Conceptualization, Methodology, Validation, Supervision. **K. Flinders:** Conceptualization, Investigation, Writing – original draft, Writing – review & editing. **D. Hancock:** Conceptualization, Investigation, Writing – original draft, Writing – review & editing. **T. Barrett:** Supervision.

Declaration of Competing Interest

The authors declare that they have no known competing financial interests or personal relationships that could have appeared to influence the work reported in this paper.

Data availability

Data will be made available on request.

Acknowledgments

The experiment was part of the EUROfusion fellowship to A. Sergis with grant agreement AWP16-ERG-CCFE. The objective of the research is to both, test and understand whether nanosuspensions could outperform conventional cooling fluids, with emphasis on Nuclear Fusion applications. The authors would like in addition to thank E. Benbow, C. Hall, F. Cismondi, B. Chuilon, D. Stone, M. Dearing, H. Lewtas for their vital assistance bringing this project forward and to conclusion as well as CCFE/UKAEA that have enabled the experiment at their HIVE facility.

References

[1] S. Xie, M.S. Beni, J. Cai, J. Zhao, Review of critical-heat-flux enhancement methods, Int. J. Heat Mass Transf. 122 (2018) 275–289, https://doi.org/10.1016/j.ijheatmasstransfer.2018.01.116.
[2] X.Q. Wang, A.S. Mujumdar, Heat transfer characteristics of nanofluids: a review, Int. J. Therm. Sci. 46 (2007) 1–19, https://doi.org/10.1016/j.ijthermalsci.2006.06.010.
[3] A. Sergis, Y. Hardalupas, Anomalous heat transfer modes of nanofluids: a review based on statistical analysis, Nanoscale Res. Lett. 6 (2011) 391, https://doi.org/10.1186/1556-276X-6-391.
[4] H. Kim, E. Kim, M.H. Kim, Effect of nanoparticle deposit layer properties on pool boiling critical heat flux of water from a thin wire, Int. J. Heat Mass Transf. 69 (2014) 164–172, https://doi.org/10.1016/j.ijheatmasstransfer.2013.10.014.
[5] S.M. You, J.H. Kim, K.H. Kim, Effect of nanoparticles on critical heat flux of water in pool boiling heat transfer, Appl. Phys. Lett. 83 (2003) 3374–3376, https://doi.org/10.1063/1.1619206.
[6] D. Hancock, Employing Additive Manufacturing for Fusion High Heat Flux Structures, The University of Sheffield, 2018.
[7] K. Kouloulias, Natural Convection and Pool Boiling Studies of Nanofluids, Imperial College London, 2018.
[8] K. Kouloulias, A. Sergis, I. Hardalupas, Optimisation of Nanofluid Properties for Reduced *In Situ* Nanoparticle Agglomeration, Universitat Jaume I, Castello, Spain, 2019.
[9] D. Taler, A new heat transfer correlation for transition and turbulent fluid flow in tubes, Int. J. Therm. Sci. 108 (2016) 108–122, https://doi.org/10.1016/j.ijthermalsci.2016.04.022.
[10] A.R. Betz, J. Xu, H. Qiu, D. Attinger, Do surfaces with mixed hydrophilic and hydrophobic areas enhance pool boiling? Appl. Phys. Lett. 97 (2010) 3–5, https://doi.org/10.1063/1.3485057.
[11] X. Chen, H. Qiu, Bubble dynamics and heat transfer on a wettability patterned surface, Int. J. Heat Mass Transf. 88 (2015) 544–551, https://doi.org/10.1016/j.ijheatmasstransfer.2015.04.086.